Efficiently Laser Driven Terahertz Surface Plasmon Polaritons on Long Metal Wire

Shuo-ting Shao,[1,*] Xiang-bing Wang,[1,*] Rong Huang,[2] Guang-yue Hu,[1,†] Min Chen,[2,‡] Hui-bo Tang,[1,3] Long-yu Kuang,[4] Yu-xi Liu,[1] Yu-qiu Gu,[4,§] Yong-kun Ding,[4,‖] Hong-bin Zhuo,[5] and Ming-yang Yu[5]

[1]*School of Nuclear Science and Technology, CAS Key Laboratory of Geospace Environment, University of Science and Technology of China, Hefei, China*

[2]*Key Laboratory for Laser Plasmas (Ministry of Education), School of Physics and Astronomy, Shanghai Jiao Tong University, Shanghai 200240, China*

[3]*School of Physics, Harbin Institute of Technology, Harbin 150001, China*

[4]*Research Center of Laser Fusion, China Academy of Engineering Physics, Mianyang, Sichuan 621900, China*

[5]*Shenzhen Key Laboratory of Ultraintense Laser and Advanced Material Technology, Center for Advanced Material Diagnostic Technology, and College of Engineering Physics, Shenzhen Technology University, Shenzhen 518118, China*

(Received 22 May 2024; accepted 20 June 2025; published 24 July 2025)

We experimentally demonstrate a novel scheme for efficiently generating intense terahertz surface plasmon polaritons (SPPs) on a subwavelength-diameter meter-long metal wire. Driven by a subrelativistic femtosecond laser ($a_0 = 0.3$, 3 mJ) focused at the wire's midpoint, single-cycle 10-MW terahertz SPPs are excited and propagate bidirectionally along it over 25 cm. The measured laser-to-SPPs energy conversion efficiency is reaching up to approximately 2.4%, which is the highest value at present. It is proved that the terahertz SPPs are excited by coherent transition radiation of the subrelativistic-laser-produced escaping electrons. Particle-in-cell together with CST simulations confirm the experimental observations. Our scheme of using readily available subrelativistic laser should thus be useful to applications requiring terawatt level single-cycle terahertz SPPs.

DOI: 10.1103/mkyj-77k8 Subject Areas: Optics, Plasma Physics, Plasmonics

I. INTRODUCTION

Intense terahertz sources [1–3] can be essential for exploring condensed-matter physics [4–6], biosensing [7–10], wireless communication [11], etc. Traditionally, generation of intense free-space terahertz radiation relies on accelerator-based relativistic electron beams that require very large facilities [12–19]. Although tabletop lasers can overcome some of the limitations, terahertz sources based on laser optical rectification [20–23] and photoconductive antennas [24,25] suffer from crystal damage. Since plasma is not damaged by intense light within the timescale of most applications, it has been invoked for generating intense terahertz pulses [26]. For example, broadband terahertz pulses can be generated by laser filamentation in gases [27–30] or liquids [31,32]. Other intense laser-plasma-interaction-based schemes using gas [33,34] or solid [35–44] targets have also been proposed, and terawatt terahertz pulses with multimillijoule energies have been demonstrated [45,46]. However, these intense free-space terahertz pulses suffer from diffraction loss and are accessible only in the line of sight, thus requiring large optical components for focusing and guiding.

Surface plasmon polaritons (SPPs) based on metal wire terahertz waveguides, which are coherent subwavelength electron oscillations localized near metal wire interfaces [47–51], allow accumulation and channeling of terahertz energy and have strong potential for realizing compact subwavelength terahertz photonics [52–57]. However, efficient coupling of metal wire-based SPPs with free-space terahertz radiation remains difficult [57]. Recently, mechanisms based on laser driven hot electrons have been proposed for directly exciting terahertz SPPs or free-space radiation on metal wires [56], including wire-guided helical undulators [58,59], SPP amplification [60], and current-carrying line antennas based on guided electrons [61] or return currents [62]. Notably, all mechanisms indicate a preference for the use of relativistic lasers to obtain intense terahertz. Moreover, there is still a lack of efficient

*These authors contributed equally to this work.
†Contact author: gyhu@ustc.edu.cn
‡Contact author: minchen@sjtu.edu.cn
§Contact author: yqgu@caep.ac.cn
‖Contact author: ding-yk@vip.sina.com

Published by the American Physical Society under the terms of the Creative Commons Attribution 4.0 International license. Further distribution of this work must maintain attribution to the author(s) and the published article's title, journal citation, and DOI.

generation and guiding mechanisms for practical applications.

In this paper, we demonstrate a novel scheme to efficiently generate single-cycle intense terahertz SPPs by focusing a subrelativistic femtosecond laser on the midsection of a meter-long subwavelength-diameter metal wire. For the first time, bidirectional electron and intense terahertz SPP propagation along the wire and emission of single-cycle terahertz radiation at the wire ends are observed, and we showed that subrelativistic, rather than relativistic (as invoked in all existing works), lasers are more suitable for exciting terahertz SPPs efficiently. This diametrically different result is attributed to coherent transition radiation (CTR) of the subrelativistic laser driven subrelativistic electrons from the long thin wire, and is confirmed by particle-in-cell and CST simulations.

II. EXPERIMENTAL SETUP

The experiments are performed in a vacuum (10^{-3} Pa pressure) chamber using a Ti:sapphire chirped-pulse amplified laser at the University of Science and Technology of China. As illustrated in Fig. 1(a), a 3-mJ, 40-fs, 790-nm, *p*-polarized subrelativistic laser pulse incidents the top center of a metal wire with 10 μm (FWHM) focal spot and 10^{17} W/cm^2 intensity (or normalized field intensity $a_0 = 0.3$). The laser contrast ratio (CR) in the nanosecond range is 10^{-8}, and each femtosecond main pulse is preceded by an approximately 40-fs prepulse with CR approximately 10^{-6} at 7 ns and a 100–500 ps-scale amplified spontaneous emission pulse with CR approximately 4×10^{-3} at 3 ns before the main pulse. The default laser incidence angle is 0°, or normal to the wire. Unless otherwise stated, tungsten wires of 30-μm diameter and 50-cm length are used. For comparison, experiments using laser incidence angles 30°, 45°, and 60°, wire diameters 50–500 μm, and wire length 1 m, as well as wire material copper, have also been carried out.

The temporal profiles of the terahertz electric field and energy of the free-space terahertz radiation at the two ends of the wire are obtained using single-shot electro-optics pump-probe technique with 1-mm-thick ZnTe crystals and 15-ps chirped probe laser [63], as well as pyroelectric detectors (Gentec-EO: THZ5B-BL-DA). The polarization and angular distribution of the terahertz pulses are measured using terahertz polarizer and continuously variable aperture combined with pyroelectric detector. High-resistance silicon wafers are placed in front of the detectors to block the infrared scattering of laser. A TPX (polymethylpentene) lens pair is used to collect the free-space terahertz radiation emitted from the wire ends and focus them onto the detectors.

The spatial distribution and energy spectra of the hot electrons at 12 cm from the laser incidence spot (LIS) guided along the wire are measured using 22×22 mm^2 fluorescent screens (DRZ-Std) and an electron magnetic spectrometer, respectively. The initial angular distribution

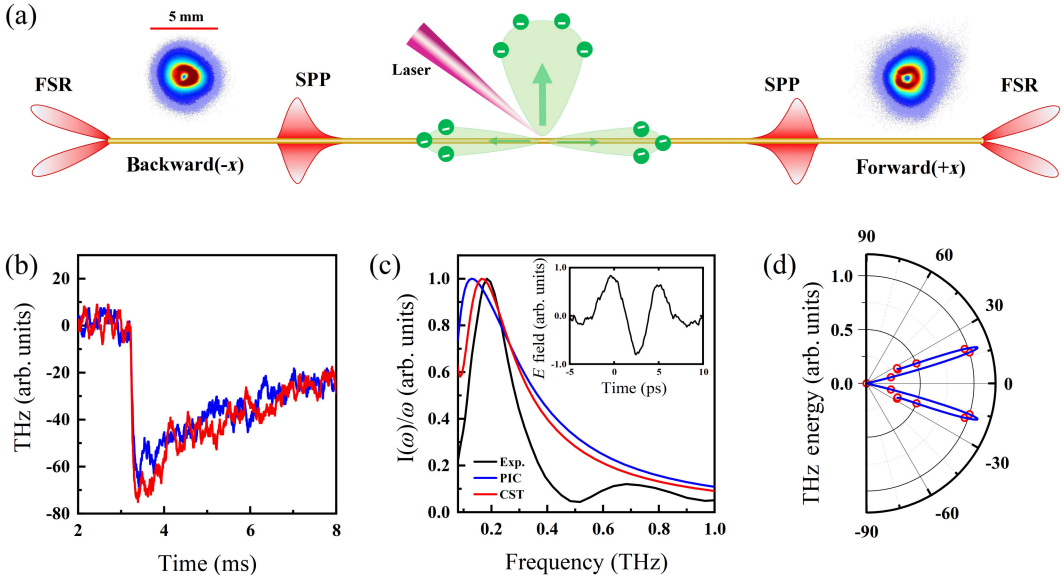


FIG. 1. (a) Result-based schematic of the experiment setup. A 3-mJ, 40-fs, subrelativistic ($a_0 = 0.3$) *p*-polarized femtosecond laser irradiates the top center of a long metal wire to expel hot electrons and generate forward and backward (in the $\pm x$ directions, respectively) propagating terahertz SPPs and electron bunches (insets, using rainbow color map), as well as free-space radiation (FSR) from the wire ends. The corresponding local electric field intensities are shown in shaded red color. (b) Energy signals of the terahertz radiation at the wire ends as detected using pyroelectric detectors. (c) Spectra and temporal profile (inset) of the terahertz SPPs from the experiment, particle-in-cell (PIC) simulation, and CST simulation. (d) Angular distribution of the terahertz emission in the horizontal plane at the wire ends as detected.

of the laser-expelled hot electrons is obtained at approximately 5 cm from the LIS using a large imaging plate (Fujifilm SR) [64], covering from −110° to +110° from the wire normal. The imaging plate is enclosed by 10-μm-thick Al foil to block low-energy x-rays and scattered light.

III. EXPERIMENTAL RESULTS

A. Characteristics of terahertz SPPs

As shown in Fig. 1(b) for the signals from the pyroelectric detectors, with normal laser incidence, the energy of the free-space terahertz radiation emitted at the ends of the wire has a typical symmetric distribution. Figure 2(a) shows that the ratio of the terahertz radiation energy of the forward ($+x$) to backward ($-x$) (F/B) is within 1 ± 0.25 from shot to shot. The inset of Fig. 1(c) shows a typical temporal terahertz electric field profile: single cycle of approximately 5-ps duration covering a broad range of frequencies up to approximately 1 THz, with central frequency at approximately 0.2 THz, or approximately 1.5 mm wavelength. Figure 1(d) for the terahertz radiation emitted from the wire ends shows that it has a hollow-cone angular distribution with approximately 20° opening angle. The polarization detector output shows that the radiation is radially polarized, suggesting that it can be a Sommerfeld surface mode on the wire [53,56,60]. The total energy of the free-space terahertz radiation emitted at the wire ends from the pyroelectric and single-shot electro-optics measurements is approximately 2×12 μJ after accounting for transmittance loss in the TPX lens and silicon wafer, and the corresponding laser-to-terahertz radiation energy conversion efficiency is approximately $2 \times 0.4\%$. Considering that most (about 2/3) of the SPPs' power is reflected at the wire ends due to impedance mismatch, the laser-to-SPP energy-conversion efficiency can be up to approximately $2 \times 1.2\%$, which is the highest value at present [see Fig. 5(a), as well as Fig. 8 and Table I in the Appendix). That is, the power of the SPPs on the wire can be more than 10 MW [56].

B. Features of guided hot electrons

The insets of Fig. 1(a) show that at 0° laser incidence, the guided hot-electron distributions in the $\pm x$ directions are symmetric. One can see that, at 12 cm from the LIS, the electrons are still localized in a ring area of outer diameter of approximately 5 mm, with the wire at the center. Such almost divergence-free guiding of laser-expelled hot electrons by thin wires has been noted earlier [66–68]. Figure 3(a) shows that these electrons have a broad (approximately 20–150 keV) energy distribution, as to be expected of laser-expelled hot electrons.

C. Nonrelevance between terahertz SPPs and guided hot electrons

Figure 2(a) shows that, even when the laser incidence angle is +45°, the bidirectional terahertz SPPs still have symmetric distribution, but the guided electrons do not: there are clearly many more electrons propagating in the backward ($-x$) direction. The guided electrons' backward-to-forward charge ratio is about 1.8 : 1 on average and can reach 8 : 1. The difference between the electron and SPP distributions confirms that the SPPs are not excited by the guided electrons, as found in several studies [58–61].

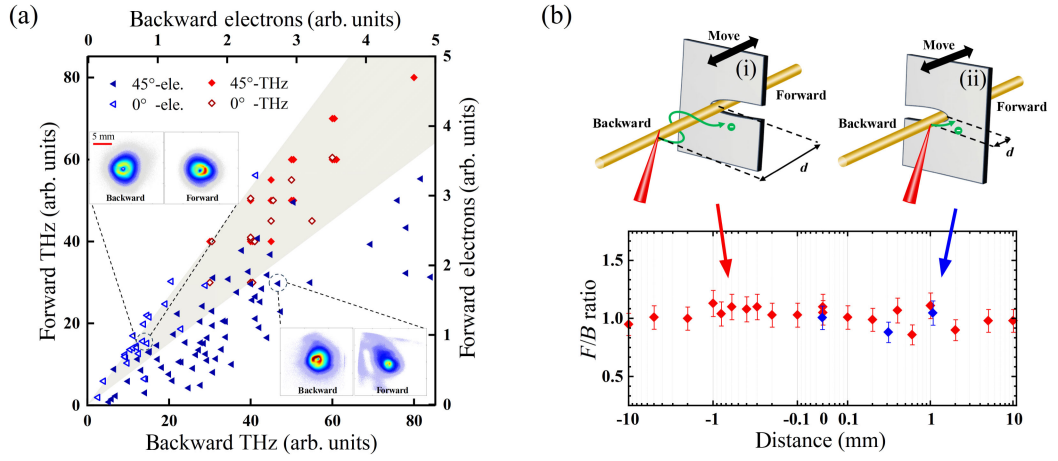


FIG. 2. (a) Energy and charge of the forward and backward ($+x$ and $-x$ directions, respectively) propagating terahertz SPPs and wire-guided electrons, respectively. The shaded area shows the range (1 ± 0.25) of the forward-to-backward (F/B) ratio. For 0° laser incidence, there are nearly the same numbers of the forward ($+x$) and backward ($-x$) propagating SPPs and electrons. For +45° laser incidence the same remains true for the SPPs, but not for the electrons. Typical distribution patterns (rainbow color scale, arbitrary units) of the electrons for 0° and +45° laser incidence are shown in the dashed lines guided upper-left and lower-right insets, respectively. (b) Ratio of the energy of the F/B propagating SPPs versus the distance between the blocking sheet and the LIS. (i) and (ii) represent electron blocking radially on the opposite side (red) and same side (blue), respectively, of the LIS on the thin wire. The error bars denote standard deviations from the measured values.

D. Manipulating the guided hot electrons

To ascertain this conclusion, additional experiments, in which the wire-guided hot electrons are artificially manipulated, have been performed. We first block the forward ($+x$) electrons with a 0.5-mm-thick Teflon sheet placed at different locations d from, and radially on the opposite side of, the LIS, as shown in Fig. 2(b)(i), and obtain the energy of the SPPs and spatial distribution of the guided electrons. When the Teflon sheet is at the rear of the laser spot, for normal laser incidence the number of forward ($+x$) moving hot electrons becomes only $1/10$ that without the Teflon sheet, but there is no change in that of the bidirectional terahertz SPPs and backward ($-x$) moving hot electrons. Similar behavior occurs when the Teflon sheet is placed from 0 to -10 mm from the LIS. (When the Teflon sheet is placed exactly at $x = 0$, the electrons moving in both directions disappear completely, while the bidirectional terahertz SPPs remain unchanged.) Thus, the wire-guided helical undulator model [58,59] and mechanisms based on laser driven hot electrons on the target backside [46,69,70] for terahertz radiation generation are not applicable to our results.

For further verification, the Teflon sheet is placed at 20 μm–1 mm from (i.e., very close to, including subterahertz-wavelength distance), and radially on the same side of, the laser spot. The laser incidence angle is changed to 45° to avoid the Teflon sheet interfering with the laser beam. Figure 2(b)(ii) shows that the forward ($+x$) hot electrons completely disappear, but the distribution patterns of the backward ($-x$) electrons and emitted terahertz pulses do not change. Thus, the models of SPP amplification [60] and current-carrying line antenna based on guided hot electrons [61] also do not apply to our results.

E. Excluding current-carrying antenna models

We also examined the applicability of the current-carrying antenna model based on return current [62]. As laser irradiates and expels hot electrons from the wire, a transient charge separation field is built up and drives return currents to its ends. Radiation from the return currents can be described by the dipole-antenna model of Smith [71]. The initial profile of the transient current is assumed to be $I_s(t) = I_0 e^{(-t^2/2\tau_0^2)}$, where I_0 and τ_0 are constants. The radiated dipole electric field is [71]

$$E(r,t) = \frac{\mu_0 c}{4\pi r}\left(\frac{\sin\phi}{1-\cos\phi}\{I_s(t-r/c) - I_s[t-r/c-(L/2c)(1-\cos\phi)]\} + \frac{\sin\phi}{1+\cos\phi}\{I_s(t-r/c) - I_s[t-r/c-(L/2c)(1+\cos\phi)]\}\right), \quad (1)$$

where ϕ is the observation angle with respect to the wire axis and L is the length of the wire. Since the radiation energy peaks in the wire-normal direction, as can be found in Fig. 6(c), coupling of the dipole radiation into SPPs on the wire is weak. Thus, the models of current-carrying line antenna based on return currents [62] also do not apply to our results.

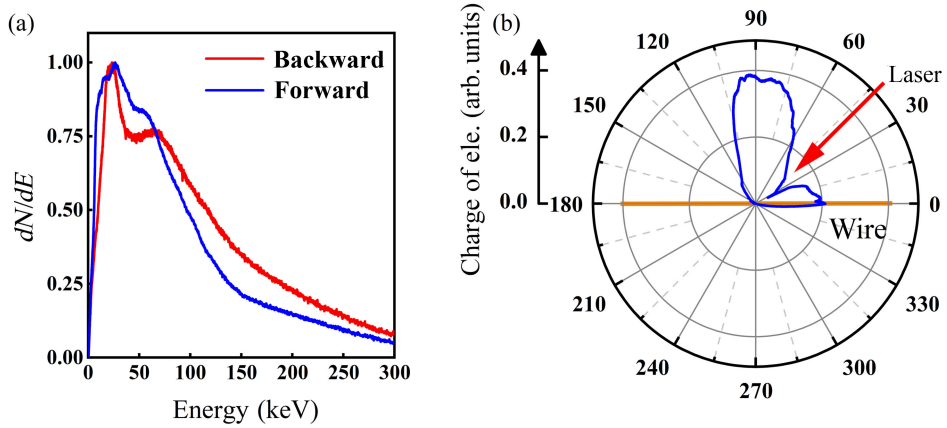


FIG. 3. Experiment results. (a) Electron energy spectra of the forward- ($+x$) and backward- ($-x$) guided hot electrons along the wire for normal (0°) laser incidence. (b) Initial angular distribution of the hot electrons near the LIS for 45° laser incidence, indicating most of the laser-expelled hot electrons there have been emitted perpendicular to the wire.

F. Measurement of expelled hot electrons

The discussions mentioned above demonstrate that the bidirectional terahertz SPPs are not produced by the guided hot electrons [58–61], the return currents [62], or the backside hot electrons [46,69,70]. We look at the initial angular distributions of the laser-expelled hot electrons there. Figure 3(b) shows that >80% of the electrons are expelled in the wire-normal direction, only a very small number are guided along the wire. Thus, the terahertz SPPs could already have been generated by the electrons ejected from the LIS in the wire-normal direction.

IV. SIMULATION AND DISCUSSION

A. Simulation setup

We use a two-dimensional PIC program from OSIRIS [72] to simulate generation of the hot electrons and terahertz SPPs. A three-dimensional finite-difference time-domain code from CST Particle Studio [73] is also used to simulate generation and delivery of terahertz SPPs. In the PIC simulation, a subrelativistic laser pulse of normalized intensity $a_0 = eE/m_e\omega c = 0.3$, wavelength $\lambda_0 = 800$ nm, FWHM duration 30 fs, and focal spot $6\lambda_0$ normally irradiates the wire at its midpoint from the top. The wire is of diameter $D = 32$ μm (or $40\lambda_0$) and density $n = 20n_c$, where n_c is the critical density. It has an inhomogeneous preplasma of width $20\lambda_0$ and scale length $L \sim 5\lambda_0$. The PIC results on the laser-expelled hot electrons are used as input in the CST simulation; namely, the transversely emitted electrons from the 30-μm-diameter main wire is of charge $0.5n_c$, pulse duration 2.4 ps, velocity $0.5c$ (or energy 80 keV), and divergence angle 30°.

B. Agreements between simulation and experiments

Our simulation results are in good agreement with that of the experiments. We found that about 88% of the total number of hot electrons are expelled in the wire-normal direction and the rest propagate along the wire in both directions, which agrees with the experiment results shown in Fig. 3(b). The spectra of the terahertz SPPs from the PIC and CST simulations shown in Fig. 1(c) also match our experiment results after convoluting the temporal resolution (approximately 800 fs) of the electro-optics measurements [74].

C. Excitation of SPPs

Figure 4 shows that a highly localized electric field is generated outside the wire by the laser-expelled electrons. (The transverse field profile shows that there is no field deep inside the thin wire centered at $r = 0$.) Radially polarized SPPs are created and propagated in both directions along the wire. The evolution is delayed if a metal wire of larger diameter is used, see Supplemental Material [65]. This scenario suggests that the SPPs are not directly excited by the laser-expelled hot electrons but are transformed from the free-space terahertz radiation produced by CTR. The CTR-produced free-space terahertz radiation is radially polarized and coupled into SPPs propagating along the wire, which is a Sommerfeld surface mode that is free from coupling loss in the transformation, as occurs in other scenarios [20,53–55].

D. Influence of electron kinetic energy

The transformation of CTR-induced terahertz radiation into SPPs free from coupling loss requires excitation by subrelativistic electrons. As illustrated in Fig. 5(a), the normalized electric field of the terahertz SPPs, obtained in our simulation and experiments, as well as previous experiments [56,58,59,62], attenuate sharply when the electron kinetic energy increases from subrelativistic (80 keV) to relativistic (3 MeV). However, under the laser intensity

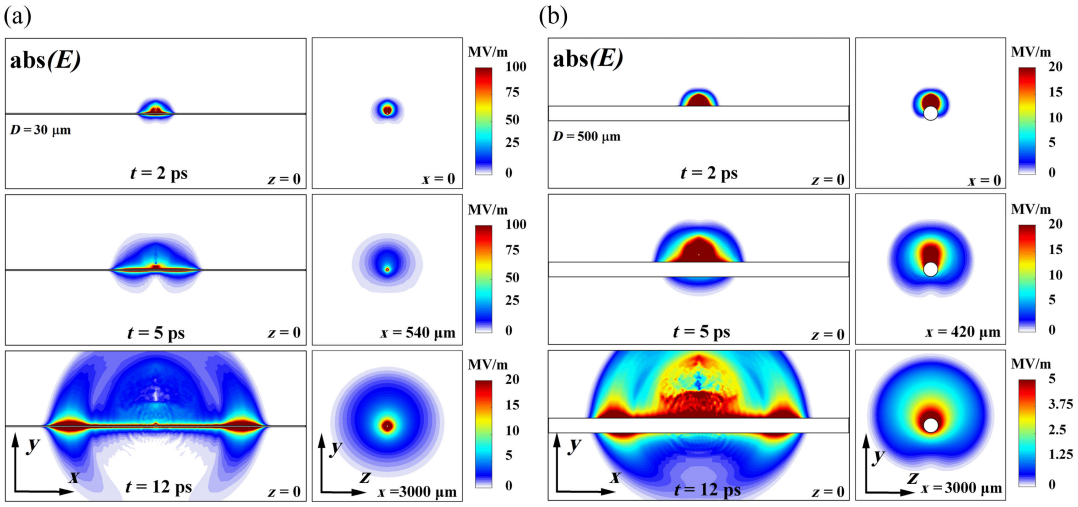


FIG. 4. CST simulation results. Evolution of the radial electric field $|E|$ [abs(E)] of the terahertz SPPs excited by the hot-electron bunches along (in the x-y plane) and transverse to (in the z-y plane) the wire axis, for wire diameters (a) $D = 30$ μm and (b) 500 μm.

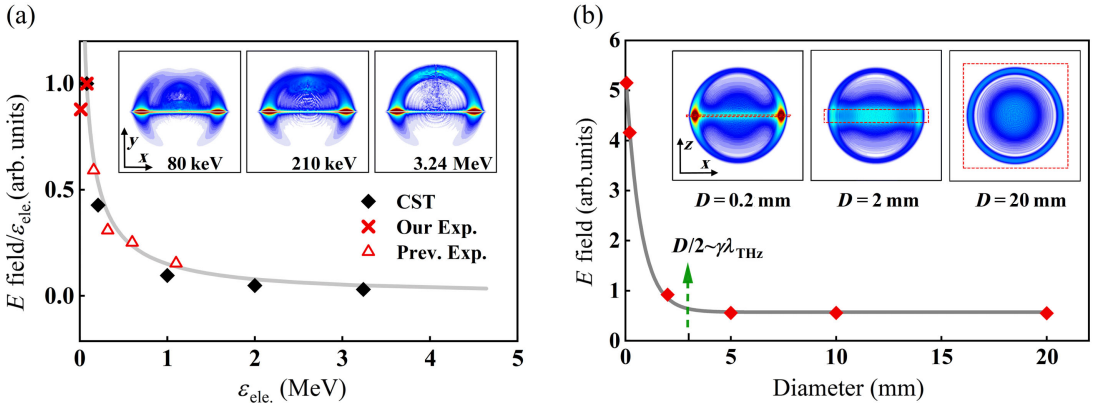


FIG. 5. (a) Dependence of the maximum electric field of the terahertz SPPs obtained in simulation (CST, at 13 ps after fast-electron ejection) and experiments (Exp.) [56,58–60,62] (normalized by electron kinetic energy ϵ_{ele}) on the electron kinetic energy fits well the analytical CTR formula integrated over the 10° segment centered at the wire axis [Eq. (2)] [75,76]. The diameter of the wire is 50 μm. The inset shows the distribution in the x-y plane of the electric field magnitude of the terahertz radiation for electron kinetic energy $\epsilon_{\mathrm{ele}} = 80$ keV, 210 keV, and 3.24 MeV. (b) Dependence of the maximum electric field of the SPPs on the wire diameter D at 25 ps after hot-electron ejection, which is well fitted by the function $1 + Ae^{-a(D/2)/\gamma\lambda}$, where the second term is from slit diffraction radiation and $\gamma\lambda \sim 1.7$ mm [78,79]. The wire cross-sectional areas are 50 μm × (0.2, 2, and 20) mm. The inset shows the distribution in the x-z plane of the electric field magnitude of the terahertz radiation. The wire boundaries are marked by red dashed lines.

dropping to 1.5×10^{16} W/cm^2, much lower laser absorption results in the terahertz energy being below the measurement threshold. A considerable part of the terahertz radiation is emitted into the free space perpendicular to the wire, which is consistent with the CTR theory that the radiation approaches the ejection direction of relativistically energetic electrons [34,39,75,76], resulting in poor coupling with the wire-guided SPPs. Since for wire length much greater than its diameter, the CTR energy spectrum in the axial direction can be expressed as (similar to that of CTR by electron beam crossing the surface of an infinite plane) [77]

$$\frac{d^2\varepsilon}{d\omega d\Omega} = \frac{N(N-1)e^2}{\pi^2 c}\left(\frac{\beta\sin\phi}{1-\beta^2\cos^2\phi}\right)^2 \times e^{-\left(\frac{2\pi}{\lambda}\right)^2\times[(a\sin\phi)^2+(\tau_e c)^2]}, \tag{2}$$

where the bunch of N electrons is of Gaussian profile in both the transverse and longitudinal directions, a and τ_e are its radius and pulse duration, respectively, β is the electron velocity normalized by the light speed, and ϕ is the observation angle. The electric field of SPPs is obtained by integrating Eq. (2) over $\phi = 0°$–$10°$ (the CTR over the angle of 10° deviates from radially polarized, impeding efficient coupling into SPPs),

$$|\boldsymbol{E}_{\mathrm{TR}}|^2 \sim \int_{\phi} \frac{d^2\varepsilon}{d\omega d\Omega}, \tag{3}$$

which fits well with the simulation and experimental results and shows that the terahertz SPPs for relativistic laser incidence [59] is of the lower conversion efficiency compared with that for subrelativistic laser incidence [58,60].

E. Effect of wire radius

We have also considered the effect of the wire radius $D/2$ on the terahertz SPPs. As shown in Fig. 5(b), the terahertz SPPs increase dramatically at $D/2 \sim \gamma\lambda \sim 1.7$ mm, since in our case the Lorentz factor is $\gamma = 1.15$ (for electron of speed $0.5c$), and the wavelength of the terahertz radiation is $\lambda = 1.5$ mm. This result is in good agreement with that of the CTR model [80–82]. When the radius of the wire is smaller than $\gamma\lambda$, i.e., comparable with that of the transverse extent of electrons' self-fields, the diffraction radiation from the wire edge can suppress the transverse CTR of the SPPs and enhance the axial CTR. The latter originates from modulation of the diffraction radiation, so that amplitude variation of the SPPs along the wire follows that of slit diffraction radiation $e^{-a(D/2)/\gamma\lambda}$ [78,79]; see Appendix C.

F. Explaining the previous experiments with CTR

Amplification of terahertz SPPs along wire reported in previous studies [58,60] can also be explained in terms of the CTR scenario here. There, diffraction radiation can also suppress the CTR along the wire. When the wire length varies from subwavelength to $\gamma\lambda$, diffraction radiation from the wire end decreases rapidly, and the CTR-generated terahertz radiation increases until the wire length reaches approximately $\gamma\lambda \sim 1.95$ mm [58] following the rule of $-e^{(-D/2)/\gamma\lambda}$. The near-field result on terahertz SPPs [60] is also consistent with that of the CTR: The radiation formation length or coherence length [39,83] is $l_f \sim \beta\lambda = 0.6$ mm since $\beta \sim 0.63$ and $\lambda = 0.94$ mm, which corresponds to the 2 ps terahertz SPPs in their experiment.

V. SUMMARY

We have considered generation and propagation of terahertz SPPs and wire-guided hot electrons on a long subwavelength-radius metal wire irradiated by subrelativistic femtosecond laser pulses. Correlation analyses of the terahertz SPPs and hot electrons show that intense terahertz SPPs can be efficiently produced from the CTR excited by the hot electrons ejected from the wire by the subrelativistic laser pulse. That is, they are not from the guided fast electrons or the return current propagating along the wire considered previously, nor from the relativistic electrons directly accelerated by a relativistic laser. The present intense terahertz SPP generation scheme has the advantage of needing only a readily available subrelativistic laser, structural simplicity, low transmission loss, and negligible group-velocity dispersion of the SPPs, as well as bidirectional delivery, so that it should be useful for integrated terahertz devices such as endoscopic terahertz systems with subwavelength spatial resolution, nonlinear terahertz pump-probe detection, waveguide-based multistage terahertz accelerators, etc. [84–88].

ACKNOWLEDGMENTS

We thank L. Q. Yi and B. F. Shen for their helpful discussions. This work was supported by the National Natural Science Foundation of China (Grants No. 12175230, No. 12225505, No. 11775223, No. 12205298), the Chinese Academy of Sciences Program for Non-Consensus and Disruptive Research (Grant No. FGSDFX-0001), and "USTC Research Funds of the Double First-Class Initiative" (Grant No. YD2140002006).

DATA AVAILABILITY

The data that support the findings of this article are openly available [89].

APPENDIX A: CURRENT-CARRYING ANTENNA MODEL

As laser irradiates the end of the wire, the guided hot electron [61] or return current [62] produces a transient current propagating along the wire to another end, which can be analyzed by a monopole-antenna model. The radiated electric field of the monopole-antenna model from Smith is [71]

$$E_{\text{monopole}}(r,t) = \frac{\mu_0 c \sin\phi}{4\pi r(1-\cos\phi)}\{I_s(t-r/c) - I_s[t-r/c-(L/2c)(1-\cos\phi)]\}, \tag{A1}$$

where ϕ is the observation angle with respect to the wire axis and L is the length of the wire. The initial profile of the transient current is assumed to be $I_s(t) = I_0 e^{(-t^2/2\tau_0^2)}$, where I_0 and τ_0 are constants.

The radiation of the monopole antenna consists of two spherical wave fronts centered at the laser irradiating spot (one end of the wire) and another wire end, shown in Fig. 6(a). The angular distribution of the radiation energy of the monopole antenna peaks closer to the wire direction, as discussed in Refs. [61,62].

However, in our experiments, the laser irradiated the midpoint of the wire, which produced double transient currents propagating toward both ends of the wire symmetrically. Thus, the radiated electric fields should be calculated using a dipole-antenna model,

$$E_{\text{dipole}}(r,t) = \frac{\mu_0 c}{4\pi r}\left(\frac{\sin\phi}{1-\cos\phi}\{I_s(t-r/c) - I_s[t-r/c-(L/2c)(1-\cos\phi)]\} + \frac{\sin\phi}{1+\cos\phi}\{I_s(t-r/c) - I_s[t-r/c-(L/2c)(1+\cos\phi)]\}\right), \tag{A2}$$

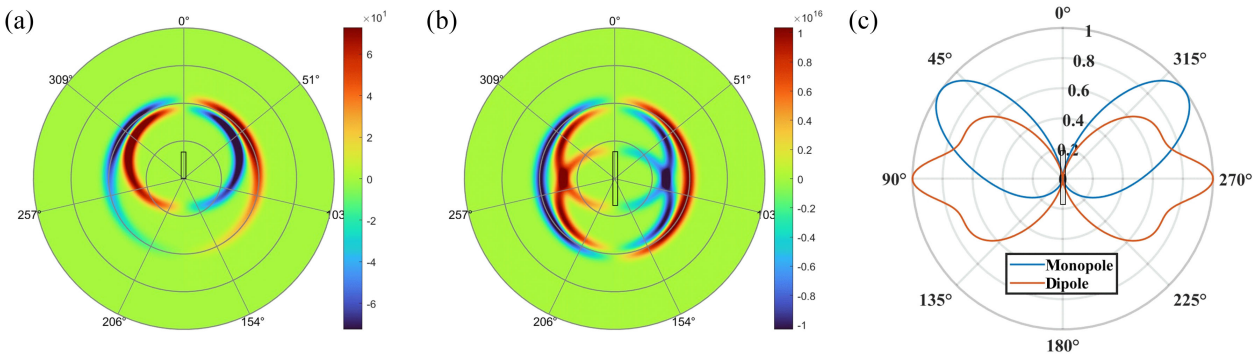


FIG. 6. Radiation electric field of line antennas at $t = 165$ fs and $L = 30$ μm. (a) The traveling wave of monopole antenna for single-ended wire. (b) The traveling wave of dipole antenna for bidirectional wire. (c) The angular distribution of radiation energy emitted by monopole and dipole antennas, respectively.

In contrast to the monopole antenna, the radiation of the dipole antenna consists of three spherical wave fronts centered at the midpoint (the laser irradiate spot) and both ends of the wire as presented in Fig. 6(b). Figure 6(c) indicates that the radiation energy from the dipole antenna peaks in the normal direction of the wire, which cannot be coupled to the SPPs on the wire. Thus, the current-carrying line antenna model does not apply to our results.

APPENDIX B: TRANSITION RADIATION AND DIFFRACTION RADIATION

Transition radiation (TR) can be generated when a perpendicularly moving charged particle crosses, stops, or starts at the interface between two media. Diffraction radiation (DR) can be emitted when a charge moves in vacuum but is close to a material surface. Coherent radiation occurs when the electromagnetic waves are generated by moving point charges within the radiation formation length, or coherence length, defined as the length of the charge path from which the generated fields arrive at the observer with nearly the same phase and are thus coherently summed.

The coherence length of TR or DR can be estimated by considering a charge moving with constant velocity $\boldsymbol{v}$ in the time interval $-T/2 < t < T/2$. The distribution of the emitted energy is [79]

$$\frac{d^2W(\boldsymbol{n},\omega)}{d\omega d\Omega} = \frac{e^2\omega^2}{4\pi^2c^3}\sqrt{\varepsilon(\omega)}[\boldsymbol{nv}]^2 \times \frac{4\sin^2[(\omega-\boldsymbol{kv})T/2]}{(\omega-\boldsymbol{kv})^2}, \tag{B1}$$

where $\boldsymbol{k} = \boldsymbol{n}k$, and $\boldsymbol{n} = \boldsymbol{r}/r$ is the wave vector of the radiation field at the observation point $\boldsymbol{r}$.

Consider the limiting case of small T, or $(\omega - \boldsymbol{kv})T \ll 1$. Equation (B1) becomes

$$\frac{d^2W(\boldsymbol{n},\omega)}{d\omega d\Omega} = \frac{e^2\omega^2}{4\pi^2c^3}\sqrt{\varepsilon(\omega)}[\boldsymbol{nv}]^2(2T)^2. \tag{B2}$$

The emitted radiation energy is proportional to T^2 and the field at the observation point is proportional to T. This is because the fields generated in a small section of the particle path arrive at the observation point with almost the same phases and are thus coherently summed. According to Eq. (B1), the radiation intensity is maximum at $T = (2N-1)\pi/(\omega - \boldsymbol{kv})$, where N is a positive integer, and is equal to zero at $T = 2N\pi/(\omega - \boldsymbol{kv})$. Thus, as vT increases, the difference between the phases of the radiation arriving at the observation point increases, so that mixing (partial cancellation) of the wave fields also increases. At $T = 2\pi/(\omega - kv)$, the fields from the two halves of the path arriving at the observation point are fully out of phase and thus cancel each other. The length of this section is

$$l_f = \frac{2\pi v}{\omega - \boldsymbol{kv}}, \tag{B3}$$

which is often referred to as the radiation formation length or the coherence length.

Therefore, coherent radiation occurs if $L \ll l_f$. The coherence length l_f varies from $\beta\lambda$ for subrelativistic electrons to $\gamma^2\lambda$ for ultrarelativistic electrons.

In the previous experiments of SPP amplification [60], 150-keV electron energy and 0.32-THz SPP frequency produce $\beta \sim 0.63$ and $\lambda \sim 0.94$ mm, respectively. The coherent length $l_f = \beta\lambda \sim 0.6$ mm implies a coherence section of 2-ps duration, which is consistent with the experimental observation.

In our case and previous experiments of helical undulators [58], which have $\beta \sim 0.5$ and $\lambda \sim 1.5$ mm for the 80-keV electron energy and 0.2-THz SPP frequency, respectively, the coherent length $l_f \sim 0.75$ mm (implies a coherence section of 2.5-ps duration) corresponds to the experimental characteristics as well.

APPENDIX C: TRANSITION RADIATION OF METAL WIRE

The transition radiation of energetic electrons expelled from a metal wire can be considered as the superposition of TR from an infinite conducting plate and DR from a slit [80–82]. As depicted in Fig. 7(a), the infinite conducting plate is located in the $x-z$ plane and the slit or wire coincides with the z axis. The electrons are normally expelled from the center of the wire along the y axis. To pass to the coordinate system including the wave vector, the system of the unit vectors is chosen as follows:

$$\begin{aligned} \boldsymbol{e_1} &= \{\cos\varphi\cos\psi, \sin\varphi\cos\psi, -\sin\psi\}, \\ \boldsymbol{e_2} &= \{-\sin\varphi, \cos\varphi, 0\}, \\ \boldsymbol{n} &= |\boldsymbol{k}|, \end{aligned} \tag{C1}$$

where ψ and φ are the polar and azimuth angles of the wave vector with respect to the z and x axis, respectively. The two components (1, 2) of the TR field in this coordinate system for the case of charge particles cross an infinite conducting plate are written in [80],

$$\begin{aligned} E_{\infty,1} &= \frac{ie}{2\pi^2}\frac{\theta_x}{(\gamma^{-2}+\theta_x^2+\theta_y^2)}, \\ E_{\infty,2} &= \frac{ie}{2\pi^2}\frac{\theta_y}{(\gamma^{-2}+\theta_x^2+\theta_y^2)}, \end{aligned} \tag{C2}$$

where γ is the Lorentz factor of the particles; $\theta_x = \pi/2 - \psi$ and $\theta_y = \pi/2 + \varphi$, respectively.

The DR field generated when the charge passes through a slit of width D (which is also the width or diameter of the wire) can be considered as a superposition of the DR fields from the upper ($\boldsymbol{E}_U$) and lower ($\boldsymbol{E}_L$) semiplanes written in the form [79]

$$\boldsymbol{E}_{\text{slit}} = \boldsymbol{E}_U e^{i\phi_U} + \boldsymbol{E}_L e^{-i\phi_L}, \tag{C3}$$

where the $\boldsymbol{E}_U$ is obtained from $\boldsymbol{E}_L$ given in Ref. [80] after the complex conjugation with simultaneous change in sign. The phase shift $\phi_U(\phi_L)$ is the radiation from the upper (lower) edge of the slit or wire with respect to the charge particle trajectory given by

$$\phi_U = \phi_L = \phi = -\frac{2\pi h}{\lambda}\cos\varphi. \tag{C4}$$

The two components (1, 2) of the DR field strength for the slit can be written as

$$E_{\mathrm{slit},1}(h) = \frac{ie}{2\pi^2}\frac{\theta_x}{(\gamma^{-2}+\theta_x^2+\theta_y^2)}\times\frac{\cos\phi\sqrt{\gamma^{-2}+\theta_x^2}+\sin\phi\theta_y}{\sqrt{\gamma^{-2}+\theta_x^2}}\times e^{-\frac{2\pi h}{\gamma\lambda}\sqrt{1+\gamma^2\theta_x^2}},$$
$$E_{\mathrm{slit},2}(h) = \frac{ie}{2\pi^2}\frac{\theta_y}{(\gamma^{-2}+\theta_x^2+\theta_y^2)}\times\frac{\cos\phi\theta_y-\sin\phi\sqrt{\gamma^{-2}+\theta_x^2}}{\theta_y}\times e^{-\frac{2\pi h}{\gamma\lambda}\sqrt{1+\gamma^2\theta_x^2}}, \tag{C5}$$

where h is the distance between the energetic electron beam and the edge of the slit or wire called the impact parameter ($h = D/2$ for defining the charge passing at the center of the slit). Consider the transversal TR and DR radiation that the radiation wave vector $\boldsymbol{k}$ directed along the x axis, so $\psi = \pi/2$ and $\varphi = 0$ corresponding to $\theta_x = 0$, $\theta_y = \pi/2$ and $\boldsymbol{e}_1 = -\boldsymbol{e}_z$, $\boldsymbol{e}_2 = \boldsymbol{e}_y$. The TR field propagating normal to the wire can be obtained using the well-known principle $\boldsymbol{E}_{\mathrm{TR},t}(h) = \boldsymbol{E}_\infty - \boldsymbol{E}_{\mathrm{slit}}(h)$ [80] as

$$E_{\mathrm{wire},t,1}(h) = -E_{t,z}(h) = 0,$$
$$E_{\mathrm{wire},t,2}(h) = E_{t,y}(h) = \frac{ie}{4\pi\gamma^{-2}+\pi^3}[1-Ce^{-\frac{2\pi h}{\gamma\lambda}}],$$
$$C = \cos\left(\frac{2\pi h}{\lambda}\right)+\frac{2}{\pi\gamma}\sin\left(\frac{2\pi h}{\lambda}\right). \tag{C6}$$

It shows that the DR from the wire edge can suppress the transversal TR due to the transversal edge effect. As can be found in Eq. (C6), the transverse radiation is out-plane polarization and will be suppressed markedly by the DR from the edge of the wire when the wire's radius is close to $\gamma\lambda$ (transverse extent of self-fields). For a round target, the edge effect exhibits as a modified Bessel function of the zeroth order $\boldsymbol{J}_0[(2\pi h)/(\gamma\lambda)]$ [39,80,83].

We found that the DR component that suppresses the transverse CTR can superpose onto the axial CTR, which enhances the radiation along the wire in our simulation, written in $E_{\mathrm{wire},a}(h) = E_\infty + AE_{\mathrm{slit},t}(h)$ with a convergence coefficient A produced by the convergence of SPP on the subwavelength-diameter wire. The $E_{\mathrm{slit},t}(h)$ is obtained by integrating Eq. (C5) over $\psi = (80°, 100°)$. We choose the plane of $\varphi = \pi/2$, so

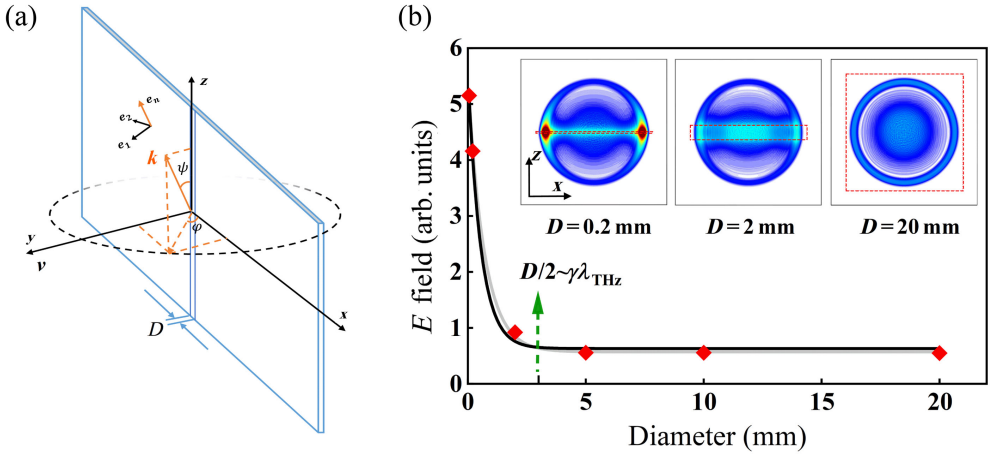


FIG. 7. (a) Geometry of the infinite plate and the slit or wire. The plate is located in the x-z plane, and the slit or wire with width D coincide with the z axis. Electron velocity $\boldsymbol{v}$ is along the y axis and $\boldsymbol{k}$ is the wave vector. (b) Dependence of the maximum electric field of the SPPs on the wire diameter D at 25 ps after hot-electron ejection, which is well fitted by the numerical solution of Eq. (C7). The function $1 + Ae^{a(-D/2)/\gamma\lambda}$ is shown with the gray curve, where the term $e^{a(-D/2)/\gamma\lambda}$ is from slit diffraction radiation and $\gamma\lambda \sim 1.7$ mm. The wire cross-sectional areas are 50 μm × (0.2, 2, and 20) mm. The inset shows the distribution in the x-z plane of the electric field magnitude of the terahertz radiation. The target boundaries are marked by red dashed lines.

the phase shift $\phi = 0$ and bring it in to derive the wire axial TR in the form of

$$E_{\mathrm{TR},a}(h) = E_\infty + A\int_\psi E_{\mathrm{slit}}d\psi, \\ \sim 1 + A\int_\psi e^{-\frac{2\pi h}{\gamma\lambda}\sqrt{1+\gamma^2\theta_x^2}}d\psi. \tag{C7}$$

As shown in Fig. 7, the axial field strength from the numerical solution of Eq. (C7) is exhibited as $1 + Ae^{-a(D/2)/\gamma\lambda}$, both fitting well with our simulation results of the dependence of maximum electric field on the wire diameter D. It shows that the influence of the DR can enhance the axial CTR when the distance between the moving charge and the wire edge (h) is smaller than $\gamma\lambda$ (transverse extent of self-fields), which occurs for $h = D/2 \sim 1.7$ mm in our case.

APPENDIX D: SUBRELATIVISTIC ELECTRONS ARE REQUIRED FOR HIGH CONVERSION EFFICIENCY

We found that subrelativistic electrons driven by a subrelativistic laser are required for efficient excitation of terahertz SPPs. To ascertain this conclusion, we collect our and previous experimental results [56,58–60,62] in Table I. Only the low-frequency radiations of <5 THz were measured in most of the experiments, thus we consider only the low-frequency component in Ref. [62] for comparison.

The experimental, simulation, and CTR analytical results are compared in Fig. 8, which shows the dependence of the electric field and the energy of terahertz on the electron kinetic energy, which have been normalized by electron energy in simulations and CTR theory, or laser energy in experiments. Experiments and simulation, as well as CTR theory exhibit the same feature: The conversion efficiency

TABLE I. Characteristics of our work and previous experiments.

	NP2017 [58]	OE2020 [59]	Nat2022 [60]	LPR2024 [62]	SR2015 [56]	Our work
Laser energy (mJ)	3	700	3	10	70	3
Peak intensity (W/cm^2)	5×10^{17}	1.95×10^{19}	1.27×10^{17}	2×10^{18}	1×10^{18}	1×10^{17}
Wire diameter (μm)	50	200	50	100	300	50
Wire length (mm)	0.1–10	100	80	0.2–6	450	250
Wire material	Metal	Tungsten	Iron	Tungsten	Tungsten	Tungsten
Terahertz energy (μJ)	28	3000	⋯	63[a]	357	40[b]
Terahertz conversion efficiency	1%	0.4%	⋯	0.63%	0.5%	1.3%[b]
Terahertz frequency	<3	<2	<1	<5[a]	<1	<5
λ_{THz} (mm)	1.5	1.7	0.94	0.6	3	1.5
Electron kinetic energy (keV)	160	1100	150	600	320	80
Electron Lorentz factor (γ,β)	(1.3, 0.65)	(3.9, 0.97)	(1.3, 0.63)	(2.2, 0.89)	(1.63, 0.78)	(1.15, 0.5)
Radiation formation length l_f [c] (mm)	0.975	25.9	0.6	0.534	2.34	0.75
Transverse extent of self-fields $\gamma\lambda_{\mathrm{THz}}$ (mm)	1.95	6.63	1.22	1.32	4.9	1.7

[a]Only the low-frequency radiation of <5 THz is considered to compare with the other experimental results.

[b]To compare with the other experimental results using short metal wire and single-directional terahertz radiation, here we account the transmission loss of terahertz SPPs on the 25-cm-length metal wire in our experiments (70%) [52,53], thus the measured 12 μJ single-directional free-space terahertz energy for long metal wire is revised to 40 μJ for short metal wire. The terahertz conversion efficiency is also revised from 0.4% for long metal wire to 1.3% for short metal wire.

[c]The radiation formation length or coherent length l_f varies from $\beta\lambda$ for subrelativistic electrons to $\gamma^2\lambda$ for ultrarelativistic electrons.

[d]When the peak laser intensity drops to 1.5×10^{16} W/cm^2 (with the estimated electron energy at 12 keV), the terahertz energy weakens to below the measurement threshold, which is approximately 0.25 μJ.

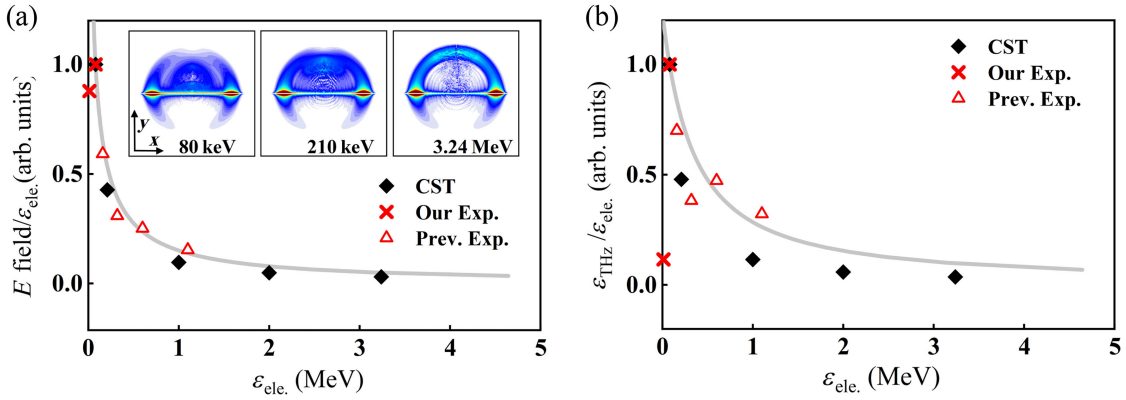


FIG. 8. (a) Dependence of the electric field of the terahertz SPPs obtained in simulation (CST, at 13 ps after fast-electron ejection) and experiments (Exp.) [56,58–60,62] (normalized by electron kinetic energy $\epsilon_{ele.}$) on the electron kinetic energy fits well the analytical CTR formula integrated over the 10° segment centered at the wire axis. The inset shows the distribution in the x-y plane of the electric field magnitude of the terahertz radiation for electron kinetic energy $\epsilon_{ele} = 80$ keV, 210 keV, and 3.24 MeV. (b) Dependence of terahertz energy (normalized by electron energy) on the electron kinetic energy, which also demonstrates well consistency between simulation, experiments, and analytical CTR formula.

from electrons or laser-to-terahertz energy decreases markedly as the electron kinetic energy increases from subrelativistic to relativistic. The slightly higher experimental results may be caused by the increased laser absorption at high light intensity [90].

[1] X. C. Zhang, A. Shkurinov, and Y. Zhang, *Extreme terahertz science*, Nat. Photonics **11**, 16 (2017).

[2] S. S. Dhillon, M. S. Vitiello, E. H. Linfield, A. G. Davies, M. C. Hoffmann, J. Booske, C. Paoloni, M. Gensch, P. Weightman, and G. P. Williams, *The 2017 terahertz science and technology roadmap*, J. Phys. D **50**, 043001 (2017).

[3] H. A. Hafez, X. Chai, A. Ibrahim, S. Mondal, D. Férachou, X. Ropagnol, and T. Ozaki, *Intense terahertz radiation and their applications*, J. Opt. **18**, 093004 (2016).

[4] M. Liu, H. Y. Hwang, H. Tao, A. C. Strikwerda, K. Fan, G. R. Keiser, A. J. Sternbach, K. G. West, S. Kittiwatanakul, J. Lu, S. A. Wolf, F. G. Omenetto, X. Zhang, K. A. Nelson, and R. D. Averitt, *Terahertz-field-induced insulator-to-metal transition in vanadium dioxide metamaterial*, Nature (London) **487**, 345 (2012).

[5] T. Kampfrath, K. Tanaka, and K. A. Nelson, *Resonant and nonresonant control over matter and light by intense terahertz transients*, Nat. Photonics **7**, 680 (2013).

[6] J. L. LaRue, T. Katayama, A. Lindenberg, A. S. Fisher, H. Öström, A. Nilsson, and H. Ogasawara, *THz-pulse-induced selective catalytic CO oxidation on Ru*, Phys. Rev. Lett. **115**, 036103 (2015).

[7] A. J. Fitzgerald, E. Berry, N. N. Zinovev, G. C. Walker, M. A. Smith, and J. M. Chamberlain, *An introduction to medical imaging with coherent terahertz frequency radiation*, Phys. Med. Biol. **47**, R67 (2002).

[8] P. Weightman, *Prospects for the study of biological systems with high power sources of terahertz radiation*, Phys. Biol. **9**, 053001 (2012).

[9] N. T. Yardimci and M. Jarrahi, *High sensitivity terahertz detection through large-area plasmonic nano-antenna arrays*, Sci. Rep. **7**, 42667 (2017).

[10] D. A. Crawley, C. Longbottom, V. P. Wallace, B. E. Cole, D. D. Arnone, and M. Pepper, *Three-dimensional terahertz pulse imaging of dental tissue*, J. Biomed. Opt. **8**, 303 (2003).

[11] S. Koenig, D. L. Diaz, J. Antes, F. Boes, R. Henneberger, A. Leuther, A. Tessmann, R. Schmogrow, D. Hillerkuss, R. Palmer, T. Zwick, C. Koos, W. Freude, O. Ambacher, J. Leuthold, and I. Kallfass, *Wireless sub-THz communication system with high data rate*, Nat. Photonics **7**, 977 (2013).

[12] N. Stojanovic and M. Drescher, *Accelerator- and laser-based sources of high-field terahertz pulses*, J. Phys. B **46**, 192001 (2013).

[13] U. Happek, A. J. Sievers, and E. B. Blum, *Observation of coherent transition radiation*, Phys. Rev. Lett. **67**, 2962 (1991).

[14] Y. Shibata, S. Hasebe, K. Ishi, T. Takahashi, T. Ohsaka, M. Ikezawa, T. Nakazato, M. Oyamada, S. Urasawa, T. Yamakawa, and Y. Kondo, *Observation of coherent diffraction radiation from bunched electrons passing through a circular aperture in the millimeter- and submillimeter-wavelength regions*, Phys. Rev. E **52**, 6787 (1995).

[15] G. L. Carr, M. C. Martin, W. R. McKinney, K. Jordan, G. R. Neil, and G. P. Williams, *High-power terahertz radiation from relativistic electrons*, Nature (London) **420**, 153 (2002).

[16] S.Bielawski, C.Evain, T.Hara, M. Hosaka, M. Katoh, S. Kimura, A. Mochihashi, M. Shimada, C. Szwaj, T. Takahashi, and Y. Takashima, *Tunable narrowband terahertz emission from mastered laser–electron beam interaction*, Nat. Phys. **4**, 390 (2008).

[17] A. M. Cook, R. Tikhoplav, S. Y. Tochitsky, G. Travish, O. B. Williams, and J. B. Rosenzweig, *Observation of narrow-band terahertz coherent Cherenkov radiation from a cylindrical dielectric-lined waveguide*, Phys. Rev. Lett. **103**, 095003 (2009).

[18] Y. Shen, X. Yang, G. L. Carr, Y. Hidaka, J. B. Murphy, and X. Wang, *Tunable few-cycle and multicycle coherent terahertz radiation from relativistic electrons*, Phys. Rev. Lett. **107**, 204801 (2011).

[19] C. Evain, C. Szwaj, E. Roussel, J. Rodriguez, M. L. Parquier, M.-A. Tordeux, F. Ribeiro, M. Labat, N. Hubert, J.-B. Brubach, P. Roy, and S. Bielawski, *Stable coherent terahertz synchrotron radiation from controlled relativistic electron bunches*, Nat. Phys. **15**, 635 (2019).

[20] J. A. Deibel, K. Wang, M. D. Escarra, and D. M. Mittleman, *Enhanced coupling of terahertz radiation to cylindrical wire waveguides*, Opt. Express **14**, 279 (2006).

[21] A. G. Stepanov, L. Bonacina, S. V. Chekalin, and J.-P. Wolf, *Generation of* 30 μJ *single-cycle terahertz pulses at 100 Hz repetition rate by optical rectification*, Opt. Lett. **33**, 2497 (2008).

[22] H. Hirori, A. Doi, F. Blanchard, and K. Tanaka, *Single-cycle terahertz pulses with amplitudes exceeding* 1 MV/cm *generated by optical rectification in LiNbO3*, Appl. Phys. Lett. **98**, 091106 (2011).

[23] M. Shalaby and C. P. Hauri, *Demonstration of a low-frequency three-dimensional terahertz bullet with extreme brightness*, Nat. Commun. **6**, 5976 (2015).

[24] D. H. Auston, K. P. Cheung, and P. R. Smith, *Picosecond photoconducting Hertzian dipoles*, Appl. Phys. Lett. **45**, 284 (1984).

[25] C. W. Berry, N. Wang, M. R. Hashemi, M. Unlu, and M. Jarrahi, *Significant performance enhancement in photoconductive terahertz optoelectronics by incorporating plasmonic contact electrodes*, Nat. Commun. **4**, 1622 (2013).

[26] G. Q. Liao and Y. T. Li, *Review of intense terahertz radiation from relativistic laser-produced plasmas*, IEEE Trans. Plasma Sci. **47**, 3002 (2019).

[27] X. Xie, J. Dai, and X.-C. Zhang, *Coherent control of THz wave generation in ambient air*, Phys. Rev. Lett. **96**, 075005 (2006).

[28] C. D'Amico, A. Houard, M. Franco, B. Prade, A. Mysyrowicz, A. Couairon, and V. T. Tikhonchuk, *Conical forward THz emission from femtosecond-laser-beam filamentation in air*, Phys. Rev. Lett. **98**, 235002 (2007).

[29] K. Y. Kim, A. J. Taylor, J. H. Glownia, and G. Rodriguez, *Coherent control of terahertz supercontinuum generation in ultrafast laser–gas interactions*, Nat. Photonics **2**, 605 (2008).

[30] M. Clerici, M. Peccianti, B. E. Schmidt, L. Caspani, M. Shalaby, M. Giguère, A. Lotti, A. Couairon, F. Légaré, T. Ozaki, D. Faccio, and R. Morandotti, *Wavelength scaling of terahertz generation by gas ionization*, Phys. Rev. Lett. **110**, 253901 (2013).

[31] I. Dey, K. Jana, V. Y. Fedorov, A. D. Koulouklidis, A. Mondal, M. Shaikh, D. Sarkar, A. D. Lad, S. Tzortzakis, A. Couairon, and G. R. Kumar, *Highly efficient broadband terahertz generation from ultrashort laser filamentation in liquids*, Nat. Commun. **8**, 1184 (2017).

[32] Q. Jin, Y. E, K. Williams, J. Dai, and X.-C. Zhang, *Observation of broadband terahertz wave generation from liquid water*, Appl. Phys. Lett. **111**, 071103 (2017).

[33] W. P. Leemans, C. G. R. Geddes, J. Faure, C. Tóth, J. van Tilborg, C. B. Schroeder, E. Esarey, G. Fubiani, D. Auerbach, B. Marcelis, M. A. Carnahan, R. A. Kaindl, J. Byrd, and M. C. Martin, *Observation of terahertz emission from a laser-plasma accelerated electron bunch crossing a plasma-vacuum boundary*, Phys. Rev. Lett. **91**, 074802 (2003).

[34] C. B. Schroeder, E. Esarey, J. van Tilborg, and W. P. Leemans, *Theory of coherent transition radiation generated at a plasma-vacuum interface*, Phys. Rev. E **69**, 016501 (2004).

[35] H. Hamster, A. Sullivan, S. Gordon, W. White, and R. W. Falcone, *Subpicosecond, electromagnetic pulses from intense laser-plasma interaction*, Phys. Rev. Lett. **71**, 2725 (1993).

[36] A. Gopal, S. Herzer, A. Schmidt, P. Singh, A. Reinhard, W. Ziegler, D. Brömmel, A. Karmakar, P. Gibbon, U. Dillner, T. May, H.-G. Meyer, and G. G. Paulus, *Observation of gigawatt-class THz pulses from a compact laser-driven particle accelerator*, Phys. Rev. Lett. **111**, 074802 (2013).

[37] G. Q. Liao *et al.*, *Bursts of terahertz radiation from large-scale plasmas irradiated by relativistic picosecond laser pulses*, Phys. Rev. Lett. **114**, 255001 (2015).

[38] A. Gopal, T. May, S. Herzer, A. Reinhard, S. Minardi, M. Schubert, U. Dillner, B. Pradarutti, J. Polz, T. Gaumnitz, M. C. Kaluza, O. Jäckel, S. Riehemann, W. Ziegler, H.-P. Gemuend, H.-G. Meyer, and G. G. Paulus, *Observation of energetic terahertz pulses from relativistic solid density plasmas*, New J. Phys. **14**, 083012 (2012).

[39] G. Q. Liao, Y. T. Li, Y. H. Zhang, H. Liu, X. L. Ge, S. Yang, W. Q. Wei, X. H. Yuan, Y. Q. Deng, B. J. Zhu, Z. Zhang, W. M. Wang, Z. M. Sheng, L. M. Chen, X. Lu, J. L. Ma, X. Wang, and J. Zhang, *Demonstration of coherent terahertz transition radiation from relativistic laser-solid interactions*, Phys. Rev. Lett. **116**, 205003 (2016).

[40] Z. Jin, H. B. Zhuo, T. Nakazawa, J. H. Shin, S. Wakamatsu, N. Yugami, T. Hosokai, D. B. Zou, M. Y. Yu, Z. M. Sheng, and R. Kodama, *Highly efficient terahertz radiation from a thin foil irradiated by a high-contrast laser pulse*, Phys. Rev. E **94**, 033206 (2016).

[41] S. Herzer, A. Woldegeorgis, J. Polz, A. Reinhard, M. Almassarani, B. Beleites, F. Ronneberger, R. Grosse, G. G. Paulus, U. Hübner, T. May, and A. Gopal, *An investigation on THz yield from laser-produced solid density plasmas at relativistic laser intensities*, New J. Phys. **20**, 063019 (2018).

[42] A. H. Woldegeorgis, B. Beleites, F. Ronneberger, R. Grosse, and A. Gopal, *Investigating the influence of incident laser wavelength and polarization on particle acceleration and terahertz generation*, Phys. Rev. E **98**, 061201(R) (2018).

[43] A. Gopal, A. Woldegeorgis, S. Herzer, and M. Almassarani, *Spatiotemporal visualization of the terahertz emission during high-power laser-matter interaction*, Phys. Rev. E **100**, 053203 (2019).

[44] A. Woldegeorgis, S. Herzer, M. Almassarani, S. Marathapalli, and A. Gopal, *Modeling terahertz emission from the target rear side during intense laser-solid interactions*, Phys. Rev. E **100**, 053204 (2019).

[45] G. Liao, Y. Li, H. Liu, G. G. Scott, D. Neely, Y. Zhang, B. Zhu, Z. Zhang, C. Armstrong, E. Zemaityte, P. Bradford, P. G. Huggard, D. R. Rusby, P. McKenna, C. M. Brenner, N. C. Woolsey, W. Wang, Z. Sheng, and J. Zhang, *Multi-millijoule coherent terahertz bursts from picosecond*

laser-irradiated metal foils, Proc. Natl. Acad. Sci. U.S.A. **116**, 3994 (2019).

[46] G. Q. Liao, H. Liu, G. G. Scott, Y. H. Zhang, B. J. Zhu, Z. Zhang, Y. T. Li, C. Armstrong, E. Zemaityte, P. Bradford, D. R. Rusby, D. Neely, P. G. Huggard, P. McKenna, C. M. Brenner, N. C. Woolsey, W. M. Wang, Z. M. Sheng, and J. Zhang, *Towards terawatt-scale spectrally tunable terahertz pulses via relativistic laser-foil interactions*, Phys. Rev. X **10**, 031062 (2020).

[47] W. L. Barnes, A. Dereux, and T. W. Ebbesen, *Surface plasmon subwavelength optics*, Nature (London) **424**, 824 (2003).

[48] X. Zhang, Q. Xu, L. Xia, Y. Li, J. Gu, Z. Tian, C. Ouyang, J. Han, and W. Zhang, *Terahertz surface plasmonic waves: A review*, Adv. Opt. Photonics **2**, 014001 (2020).

[49] P. Berini and I. De Leon, *Surface plasmon-polariton amplifiers and lasers*, Nat. Photonics **6**, 16 (2012).

[50] *Surface Plasmon Nanophotonics*, edited by M. L. Brongersma and P. G. Kik (Springer, Dordrecht, 2007).

[51] *Handbook of Terahertz Technology for Imaging, Sensing and Communications*, edited by D. Saeedkia (Woodhead Publishing, 2013), https://api.semanticscholar.org/CorpusID:106872495.

[52] K. Wang and D. M. Mittleman, *Metal wires for terahertz wave guiding*, Nature (London) **432**, 376 (2004).

[53] K. Wang and D. M. Mittleman, *Guided propagation of terahertz pulses on metal wires*, J. Opt. Soc. Am. B **22**, 2001 (2005).

[54] W. Op't Root, G. Brussaard, P. Smorenburg, and O. Luiten, *Single-cycle surface plasmon polaritons on a bare metal wire excited by relativistic electrons*, Nat. Commun. **7**, 13769 (2016).

[55] P. W. Smorenburg, W. P. E. M. Op't Root, and O. J. Luiten, *Direct generation of terahertz surface plasmon polaritons on a wire using electron bunches*, Phys. Rev. B **78**, 115415 (2008).

[56] S. Tokita, S. Sakabe, T. Nagashima, M. Hashida, and S. Inoue, *Strong sub-terahertz surface waves generated on a metal wire by high-intensity laser pulses*, Sci. Rep. **5**, 8268 (2015).

[57] K. Teramoto, S. Inoue, S. Tokita, R. Yasuhara, Y. Nakamiya, T. Nagashima, K. Mori, M. Hashida, and S. Sakabe, *Induction of subterahertz surface waves on a metal wire by intense laser interaction with a foil*, Phys. Rev. E **97**, 023204 (2018).

[58] Y. Tian, J. S. Liu, Y. F. Bai, S. Y. Zhou, H. Y. Sun, W. W. Liu, J. Y. Zhao, R. X. Li, and Z. Z. Xu, *Femtosecond-laser-driven wire-guided helical undulator for intense terahertz radiation*, Nat. Photonics **11**, 242 (2017).

[59] Y. Zeng, C. Zhou, L. Song, X. Lu, Z. Li, Y. Ding, Y. Bai, Y. Xu, Y. Leng, Y. Tian, J. Liu, R. Li, and Z. Xu, *Guiding and emission of milijoule single-cycle THz pulse from laser-driven wire-like targets*, Opt. Express **28**, 15258 (2020).

[60] D. D. Zhang, Y. S. Zeng, Y. F. Bai, Z. P. Li, Y. Tian, and R. X. Li, *Coherent surface plasmon polariton amplification via free-electron pumping*, Nature (London) **611**, 55 (2022).

[61] H. B. Zhuo, S. J. Zhang, X. H. Li, H. Y. Zhou, X. Z. Li, D. B. Zou, M. Y. Yu, H. C. Wu, Z. M. Sheng, and C. T. Zhou, *Terahertz generation from laser-driven ultrafast current propagation along a wire target*, Phys. Rev. E **95**, 013201 (2017).

[62] J. Wang, Z. Zhang, S. Zhou, Z. Qin, C. Yu, Y. Cao, Y. Lv, J. Chen, H. Huang, W. Liu, and J. Liu, *Radiation dynamics and manipulation of extreme terahertz surface wave on a metal wire*, Laser Photonics Rev. **19**, 2400954 (2025).

[63] Z. P. Jiang and X.-C. Zhang, *Electro-optic measurement of THz field pulses with a chirped optical beam*, Appl. Phys. Lett. **72**, 1945 (1998).

[64] T. Bonnet, M. Comet, D. D. Petit, F. Gobet, F. Hannachi, M. Tarisien, M. Versteegen, and M. M. Aléonard, *Response functions of imaging plates to photons, electrons and* ^{4}He *particles*, Rev. Sci. Instrum. **84**, 103510 (2013).

[65] See Supplemental Material at http://link.aps.org/supplemental/10.1103/mkyj-77k8 for the excitation and evolution of SPPs.

[66] R. Kodama *et al.*, *Plasma devices to guide and collimate a high density of MeV electrons*, Nature (London) **432**, 1005 (2004).

[67] S. Tokita, K. Otani, T. Nishoji, S. Inoue, M. Hashida, and S. Sakabe, *Collimated fast electron emission from long wires irradiated by intense femtosecond laser pulses*, Phys. Rev. Lett. **106**, 255001 (2011).

[68] H. Nakajima, S. Tokita, S. Inoue, M. Hashida, and S. Sakabe, *Divergence-free transport of laser-produced fast electrons along a meter-long wire target*, Phys. Rev. Lett. **110**, 155001 (2013).

[69] J. Déchard, X. Davoine, L. Gremillet, and L. Bergé, *Terahertz emission from submicron solid targets irradiated by ultraintense femtosecond laser pulses*, Phys. Plasmas **27**, 093105 (2020).

[70] E. Denoual, L. Bergé, X. Davoine, and L. Gremillet, *Modeling terahertz emissions from energetic electrons and ions in foil targets irradiated by ultraintense femtosecond laser pulses*, Phys. Rev. E **108**, 065211 (2023).

[71] G. S. Smith, *An Introduction to Classical Electromagnetic Radiation* (Cambridge University Press, Cambridge, England, 1997), https://api.semanticscholar.org/CorpusID:118583453.

[72] R. A. Fonseca, L. O. Silva, F. S. Tsung, V. K. Decyk, W. Lu, C. Ren, W. B. Mori, S. Deng, S. Lee, T. Katsouleas, and J. C. Adam, *Computational Science—ICCS 2002*, edited by P. M. A. Sloot, A. G. Hoekstra, C. J. K. Tan, and J. J. Dongarra (Springer, Berlin Heidelberg, 2002), Vol. 2331, pp. 342–351, 10.1007/3-540-47789-6.

[73] *CST Particle Studio*, http://www.cst.com/products/cstps.

[74] F. G. Sun, Z. Jiang, and X. C. Zhang, *Analysis of terahertz pulse measurement with a chirped probe beam*, Appl. Phys. Lett. **73**, 2233 (1998).

[75] W. J. Ding and Z. M. Sheng, *Sub GV/cm terahertz radiation from relativistic laser-solid interactions via coherent transition radiation*, Phys. Rev. E **93**, 063204 (2016).

[76] J. Zheng, K. A. Tanaka, T. Miyakoshi, Y. Kitagawa, R. Kodama, T. Kurahashi, and T. Yamanaka, *Theoretical study of transition radiation from hot electrons generated in the laser–solid interaction*, Phys. Plasmas **10**, 2994 (2003).

[77] J. Zheng, K. A. Tanaka, T. Miyakoshi, Y. Kitagawa, R. Kodama, T. Kurahashi, and T. Yamanaka, *Spectrum of transition radiation from hot electrons generated in*

ultra-intense laser plasma interaction, Phys. Plasmas **9**, 3610 (2002).

[78] D. V. Karlovets and A. P. Potylitsyn, *On the theory of diffraction radiation*, J. Exp. Theor. Phys. **107**, 755 (2008).

[79] A. P. Potylitsyn, M. I. Ryazanov, M. N. Strikhanov, and A. A. Tishchenko, *Diffraction Radiation from Relativistic Particles* (Springer, Berlin, Heidelberg, 2011).

[80] A. Potylitsyn, *Transition radiation and diffraction radiation. similarities and differences*, Nucl. Instrum. Methods Phys. Res., Sect. B **145**, 169 (1998).

[81] A. Tishchenko, M. Strikhanov, and A. Potylitsyn, *X-ray transition radiation from an ultrarelativistic charge passing near the edge of a target or through a thin wire*, Nucl. Instrum. Methods Phys. Res., Sect. B **227**, 63 (2005).

[82] N. F. Shul'ga and S. N. Dobrovol'skii, *Theory of relativistic-electron transition radiation in a thin metal target*, J. Exp. Theor. Phys. **90**, 579 (2000).

[83] L. C. L. Yuan, C. L. Wang, H. Uto, and S. Prünster, *Formation-zone effect in transition radiation due to ultrarelativistic particles*, Phys. Rev. Lett. **25**, 1513 (1970).

[84] E. A. Nanni, W. R. Huang, K. H. Hong, K. Ravi, A. Fallahi, G. Moriena, R. J. D. Miller, and F. X. Kärtner, *Terahertz-driven linear electron acceleration*, Nat. Commun. **6**, 8486 (2015).

[85] D. F. Zhang, A. Fallahi, M. Hemmer, X. Wu, M. Fakhari, Y. Hua, H. Cankaya, A. L. Calendron, L. E. Zapata, N. H. Matlis, and F. X. Kärtner, *Segmented terahertz electron accelerator and manipulator (STEAM)*, Nat. Photonics **12**, 336 (2018).

[86] E. Curry, S. Fabbri, J. Maxson, P. Musumeci, and A. Gover, *Meter-scale terahertz-driven acceleration of a relativistic beam*, Phys. Rev. Lett. **120**, 094801 (2018).

[87] C. Kealhofer, W. Schneider, D. Ehberger, A. Ryabov, F. Krausz, and P. Baum, *All-optical control and metrology of electron pulses*, Science **352**, 429 (2016).

[88] L. Zhao *et al.*, *Terahertz streaking of few-femtosecond relativistic electron beams*, Phys. Rev. X **8**, 021061 (2018).

[89] S. Shao, Zenodo, 10.5281/zenodo.15364016 (2025).

[90] Y. Ping, R. Shepherd, B. F. Lasinski, M. Tabak, H. Chen, H. K. Chung, K. B. Fournier, S. B. Hansen, A. Kemp, D. A. Liedahl, K. Widmann, S. C. Wilks, W. Rozmus, and M. Sherlock, *Absorption of short laser pulses on solid targets in the ultrarelativistic regime*, Phys. Rev. Lett. **100**, 085004 (2008).